RSC Advances

PAPER

View Article Online
View Journal | View Issue

Cite this: *RSC Adv.*, 2025, **15**, 10426

A tailored 4G *s*-triazine-based dendrimer vehicle for quercetin endowed with MMP-2/9 inhibition and VEGF downregulation for targeting breast cancer progression and liver metastasis†

Doaa R. Ramadan, *[a] Heba A. Osman,[b] Somaya Aly Madhy,[a] Mohamed Teleb,[cd] A. I. Darwish,[b] Marwa M. Abu-Serie,[e] Nesreen S. Haiba,[b] Sherine N. Khattab*[a] and Hosam H. Khalil[a]

Received 5th March 2025
Accepted 24th March 2025

DOI: 10.1039/d5ra01588j

rsc.li/rsc-advances

Motivated by our recent research progress on the exploitation of *s*-triazine dendritic platforms as bioactive carriers for well-known anticancer agents and/or targeting ligands, we set out to synthesize new rationally designed dendrimers endowed with MMP-2/9 inhibition potential for halting both breast and liver cancer progression with reduced off-target side effects. New three and four generation *s*-triazine based dendrimers were developed to incorporate potential ZBGs (Zinc Binding Groups) and carboxyl terminal groups to facilitate direct conjugation of anti-cancer drugs (quercetin) and/or targeting ligands (lactobionic acid) through a biodegradable ester bond. Compared to free quercetin (QUR), MTT assay revealed that all the quercetin-coupled dendrimers displayed better anticancer potential (IC_{50} = 12.690–29.316, 4.137–29.090 μM) against MCF-7 and HepG-2 cancer cells, respectively within their safe doses (EC_{100} = 134.35–78.44 μM). Conjugation of lactobionic acid and PEG boosted the anticancer potency against both treated cells, improved apoptosis and down regulated MMP-9 and VEGF gene expression levels in both treated cancer cells. Generally, the more branched **G4** dendrimer conjugates exhibited a superior overall anticancer performance compared to their respective **G3** analogues, except for their MMP-9 inhibition where **G3** conjugate appeared to be more potent and more selective than its **G4** analogue.

1. Introduction

The GLOBOCAN 2020 statistics released by the International Agency for Research on Cancer (IARC) have reported the worst incidence rates of breast cancer in 185 countries. Breast cancer is considered the leading most diagnosed cancer. It is estimated that one in 4 women is suffering from breast cancer, and one in 8 women died due to it.[1] The global breast cancer burden is estimated to reach 28.4 million cases by 2040, which is approximately a 47% raise compared to the 2020 cancer burden.[2] Distant metastases are also considered the main reason for mortalities associated with breast tumors. The liver is one of the most common sites of breast cancer metastases that is difficult to prognose with an average survival time of 2–3 years.[3] Liver metastases develop in about half of patients diagnosed with metastatic breast cancer. It is also a common location for tumor reoccurrence in about 5–12% of those people.[4] Insufficiency of an adequate approach for early diagnosis and effective therapy remains crucial for high mortality especially in developing countries,[5] posing the necessity to develop innovative targeted breast cancer therapy that can also limit liver metastasis. Recently, the breast cancer microenvironment, particularly the altered extracellular matrix, has been recognized as a critical element that fosters both tumor development and metastasis[6] *via* a plethora of proteinases.[7–9] Most importantly, matrix metalloproteinases (MMPs) promote extracellular matrix turnover, cancer cell proliferation, and metastasis, thus viewed as the major modulators of the tumor microenvironment.[10–12] Dysregulation of MMPs has been reported in most tumors.[13–15] The MMPs family includes 26 structurally-related zinc-dependent endopeptidases[16] classified

[a]*Chemistry Department, Faculty of Science, Alexandria University, Alexandria 21321, Egypt. E-mail: doaareda@alexu.edu.eg; doaareda.ramadan@unimi.it; Sh.n.khattab@gmail.com; sherinekhattab@alexu.edu.eg*

[b]*Department of Physics and Chemistry, Faculty of Education, Alexandria University, Alexandria, Egypt*

[c]*Department of Pharmaceutical Chemistry, Faculty of Pharmacy, Alexandria University, Alexandria 21521, Egypt*

[d]*Cancer Nanotechnology Research Laboratory (CNRL), Faculty of Pharmacy, Alexandria University, Alexandria 21521, Egypt*

[e]*Medical Biotechnology Department, Genetic Engineering and Biotechnology Research Institute, City of Scientific Research and Technological Applications (SRTA-City), Alexandria, Egypt*

† Electronic supplementary information (ESI) available. See DOI: https://doi.org/10.1039/d5ra01588j

as: collagenases, gelatinases, stromelysins, matrilysins, membrane-type MMPs, and others.[17] Various members of the MMPs family have been validated as anticancer targets.[18–21] Early studies utilized peptidomimetics of endogenous ligands capped with the hydroxamate zinc-binding group (ZBG) as potential inhibitors.[21] However, the clinical failure[22] of hydroxamates due to off-target side effects[18–24] and pharmacokinetic challenges[25,26] then directed design strategies to ZBG diversification. In this regard, carboxylates, hydrazides, *N*-hydroxyurea, thiols, sulfonylhydrazides, and others were introduced as MMP inhibitors.[27] However, this approach did not guarantee clinical success so far due to a lack of selectivity.[25–28]

On the other hand, a fundamentally different strategy was adopted aided with computational studies for developing inhibitors lacking ZBGs for avoiding zinc binding-related off-target side effects.[29–32] Despite being successful, this strategy was only suitable for developing inhibitors of the deep-pocket MMPs isoforms, particularly MMP-13, where the inhibitor's fitting is mainly dependent on the intrinsic flexibility of the MMP specificity loop. Therefore, such inhibitors selectivity against other MMPs seems to be questionable. Collectively, the aforementioned challenges raised a dilemma about the design strategy; "to bind zinc for potency or not to bind zinc for selectivity?".[13] A pragmatic solution for achieving the optimum selectivity and potency compromise may be through targeting the tumor microenvironment itself. A recent study demonstrated that targeted delivery of the hydroxamate peptidomimetic MMP inhibitor marimastat encapsulated in thermosensitive liposomes to the tumor microenvironment enhanced MMP-2 and MMP-9 inhibition with reduced off-target effects.[33] Monoclonal antibodies were also utilized for targeting specific MMPs catalytic domains without zinc binding,[34] such as DX-2400 innovated by Dyax that selectively inhibited MMP-14 and limited liver and lung cancers metastases.[35] Gilead Sciences also introduced the humanized monoclonal antibody Andecaliximab (GS-5745) as selective MMP-9 inhibitor that hindered tumor progression without side effects.[36] Dendrimer-based nanotherapeutics have emerged as a prominent focus of research,[37–40] largely due to their tree-like structure that can accommodate different molecules such as drugs, targeting agents, and even imaging entities. These molecules can be physically encapsulated within the pores of the dendritic structure or chemically conjugated to the dendrimer's peripheries through a biodegradable bond that responds to a specific pH, temperature, or enzyme present in the tumor microenvironment.[41–43] In addition, physical aspects of the dendritic nanoparticles can be meticulously controlled to optimize their pharmacokinetics ensuring higher tumor accumulation of anti-cancer agents.[44] The use of dendrimers in targeted drug delivery is often likened to a "Trojan horse" strategy,[45] offering a highly tailored approach to efficiently and selectively transport pharmacophores to targeted tumor cells. Several strategies have been reported on the use of dendrimers and other polymeric nanoparticles to efficiently induce anti-cancer activity through MMPs inhibition.[46–48] Pioneer targeting strategies utilized dendrimers decorated with pharmacophoric entities, thus rendering them "drug-like",[37,49–55] besides being amenable to functionalization[56,57] with targeting ligands that deliver their bioactive payloads to the target locus.[58] This "out of the box" approach directed synthetic protocols to rationally functionalize some poly(amidoamine) PAMAM dendrimers"[49–52] and triazine-based ones to act as MMP inhibitors.[59–61] Driven by our recent work in exploring *s*-triazine dendritic platforms as bioactive carriers for established anticancer agents and targeting ligands,[60,61] we embarked on the synthesis of novel, strategically designed dendrimers. These dendrimers are specifically engineered to exhibit potent inhibition of MMP-2/9, aiming to effectively halt the progression of both breast and liver cancer while minimizing off-target side effects.

2. Design rationale

Inspired by the multifaced design approach utilizing dendrimers in MMP research, the current study portrays engineering breast cancer-targeted triazine-based dendrimers (Fig. 1) endowed with MMP inhibitory potential, especially MMP-9 being highly expressed in breast cancer[62,63] and closely related to liver metastasis and tumor staging.[64,65] Firstly, we built four generations of *s*-triazine dendrimers with phenylene diamine core and glycine branching linkers, decorated with carboxylic acids warheads as potential ZBGs for guaranteed significant MMP inhibitory potential. The prepared dendrimers were screened for their possible cytotoxic activities on normal human fibroblasts (Wi-38) to evaluate their safety profiles utilizing MTT assay.[66] As a proof of concept, the dendrimers were subsequently subjected to *in vitro* MMP-9 inhibition assay compared to the reference MMP inhibitor *N*-isobutyl-*N*-(4-methoxyphenylsulfonyl)glycyl hydroxamic acid (NNGH). Their selectivity profiles towards MMP-9 over the closely related MMP-2 were assigned. The bioactive *s*-triazine dendritic scaffolds were then utilized as targeted carriers for rationalized therapeutic payloads and targeting ligands. Herein, the free acid-terminated dendrimers were directly conjugated to quercetin (QUR), a multitarget anticancer phytochemical flavonoid that efficiently inhibits MMP-9,[67] followed by coupling of lactobionic acid (LA), a biocompatible[68] targeting ligand that can be recognized by the asialoglycoprotein receptors (ASGPR) overexpressed on liver and breast tumorous tissues.[69–71] Furthermore, the chosen targeting ligand exhibits MMP inhibitory potential,[72,73] offering additional opportunity to synergize with the MMP inhibitory activities of the free dendrimers and QUR, potentiating the overall potency of the conjugated system. Finally, the synthesized dendrimer conjugates were PEGylated through a biodegradable ester bond to improve their pharmacokinetics and safety profiles.[74] All the synthesized dendritic conjugates were subjected to MTT assay[66] to assess their cytotoxicity on normal fibroblasts (Wi-38), breast cancer cells (MCF-7) and liver cancer cells (HepG-2). Moreover, their apoptotic induction potential in comparison to QUR based on earlier studies reporting the apoptotic effects of QUR in breast[75] and liver[76] cancers, as well as related studies illustrating the role of MMP-9 inhibitors in enhancing tumor cell apoptosis.[77] The biological evaluation was extended to investigate the regulatory effect of the synthesized dendrimeric conjugates on VEGF

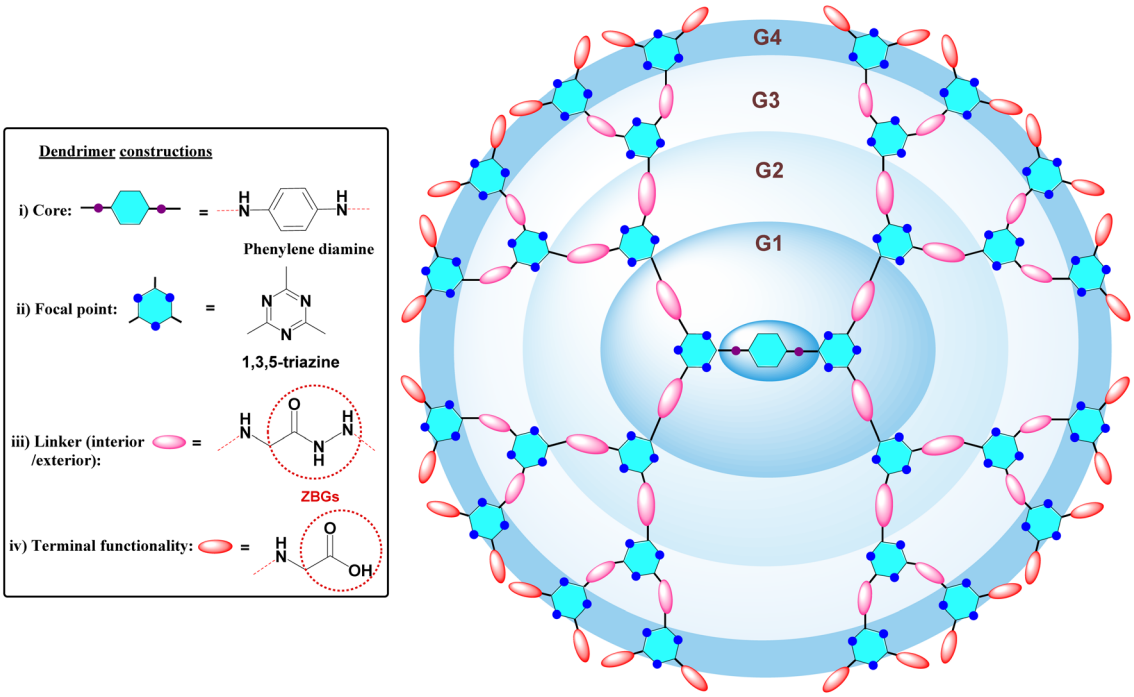

Fig. 1 Design for targeted *s*-triazine-based dendrimer with phenylene diamine core, branching glycine linkers and customizable carboxyl termini.

expression being identified as one the most critical signaling pathways regulating breast cancer liver metastasis.[78]

3. Results and discussion

3.1. Chemistry

3.1.1. Divergent synthesis of G1–G4 triazine-dendrimers. A simple synthetic strategy was adapted to grow the generations of the designed *s*-triazine dendrimers, where we took advantage of the temperature-dependent sequential nucleophilic substitution of the tri-functional trichloro *s*-triazine **1** to build our targeted dendrimer scaffolds. In fact, two types of nucleophilic substitution reactions were performed iteratively during the preparation of these dendrimers: (1) nucleophilic aromatic substitution of chlorine atoms from *s*-triazine derivatives and (2) acyl nucleophilic substitution reactions during functional group transformation from acid to ester then finally to hydrazide derivatives.

3.1.2. Synthesis of repeating units 3 and 4 for the designed dendrimers. To construct the designed dendritic architecture, first the repeating units **3** and **4** had to be synthesized following the same previously reported procedure[60,79,80] by reaction of cyanuric chloride **1** with two equivalents of glycine **2** to afford disubstituted cyanuric chloride **3**, then the obtained monochlorinated triazine **3** was reacted with hydrazine hydrate at room temperature to afford the corresponding hydrazine derivative **4** (Scheme 1). The spectral data of **3** and **4** were consistent with the literature.[60] These two units will be utilized later to grow the targeted different generation dendrimers.

3.1.3. Synthesis of 1st generation dendrimer with a phenylene diamine core. The first generation triazine dendrimer (TPhyG$_1$-OH) **6** was prepared by nucleophilic aromatic substitution of Cl-atoms in two molecules of the monochlorinated triazine monomer **3** by the amino groups of *p*-phenylene diamine **5**.[80] The reaction mixture was refluxed for 10 h, to ensure the substitution of the less reactive third chlorine atom, in presence of sodium carbonate, to scavenge the liberated HCl. This reaction afforded the dimer TPhyG$_1$-OH **6** which will be the core of our targeted dendritic structure (Scheme 2). To build the next generation of the dendrimer, the terminal carboxyl groups of the core TPhyG$_1$-OH **6** must be transformed into nucleophilic

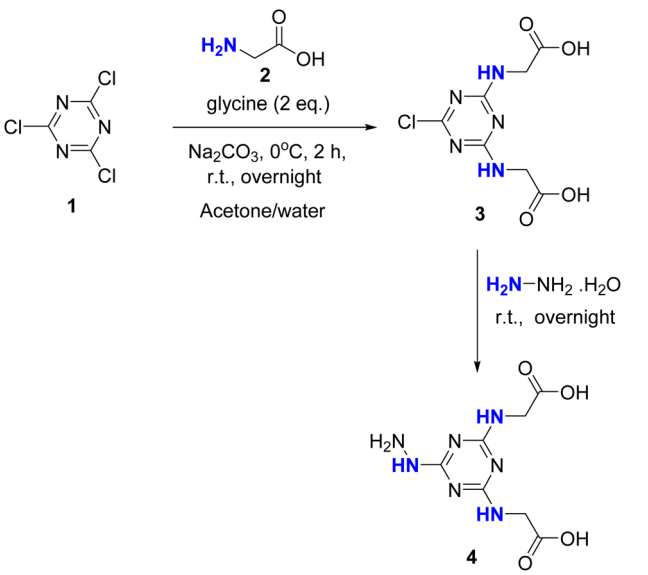

Scheme 1 Synthesis of repeating units **3** and **4**.

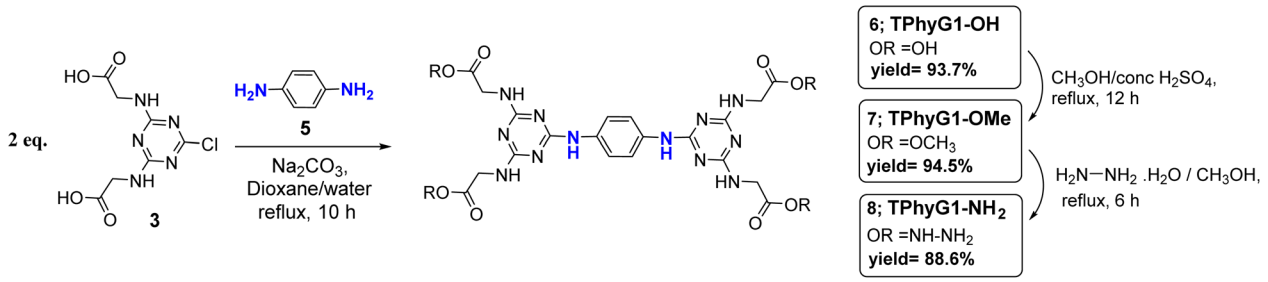

Scheme 2 Synthesis of first generation of triazine dendrimer (TPhyG$_1$-OH) **6**, their methyl ester (TPhyG$_1$-OMe) **7** and hydrazide derivative (TPhyG$_1$-NH$_2$) **8**.

groups so that it can be connected to another monochlorinated triazine repeating unit. This is achieved by esterification of the carboxylic acid end groups of TPhyG$_1$-OH **6** in methanol to give the corresponding methyl ester TPhyG$_1$-OMe **7** which is subsequently reacted with hydrazine hydrate to produce the corresponding hydrazide derivative TPhyG$_1$-NH$_2$ **8** with four nucleophilic NH–NH$_2$ end groups (Scheme 2).[80] This transformation was confirmed by IR spectra where the broad band of OH bond in TPhyG$_1$-OH **6** and the NH$_2$ absorption in TPhyG$_1$-NH$_2$ **8** were identified. While the IR spectrum of the ester TPhyG$_1$-OMe **7** showed the C=O absorption band at 1743 cm^{-1}. The ^{1}H-NMR spectra of both TPhyG$_1$-OH **6** and TPhyG$_1$-NH$_2$ **8** in D$_2$O showed a multiplet peak at chemical shift 3.80–4.10 ppm corresponding to the four α-CH$_2$ protons of the glycine residue and another at 7.10–7.30 ppm corresponding to the four aromatic protons of the phenylene ring, confirming the formation of the dimer. Whereas the ^{1}H-NMR spectrum of the respective ester TPhyG$_1$-OMe **7** showed an additional multiplet peak at 3.58–3.72 ppm corresponding to OMe protons. The ^{13}C-NMR spectrum of **7** also confirms the presence of methoxy groups.

3.1.4. Synthesis of 2nd generation dendrimers. **G2** dendrimer TPhyG$_2$-OH **9** was synthesized following two strategies, the first one utilizes nucleophilic substitution of 4 equivalents of the monochlorinated *s*-traizine derivative **3** by the tetrahydrazide-terminated **G1** dendrimer TPhyG$_1$-NH$_2$ **8** (Scheme 3, route i). Thus, growing another generation with four more repeating units attached to the peripheries of the starting **G1** dendrimer **8**. The second strategy involves nucleophilic acyl substitution of the four ester end groups of TPhyG$_1$-OMe **7** by NH$_2$ functional group of the trisubstituted *s*-triazine repeating unit **4** (Scheme 3, route ii) affording the same 2nd generation dendrimer TPhyG$_2$-OH **9**, with eight carboxyl terminal groups. The first synthetic method appears to be more effective, affording the desired G2 dendrimer **9** in a higher yield (~81%). The success of forming the second generation was confirmed by the ^{1}H-NMR of **9**, where a notable increase in the integration of CH$_2$ peaks is found as it corresponds to 4 internal α-CH$_2$ and 8 external α-CH$_2$ of the glycine residues, while no change is observed in the aromatic region corresponding to 4 protons of the phenylene diamine core. The corresponding G2 dendrimer analogues **10** and **11** were achieved by esterification of the acid

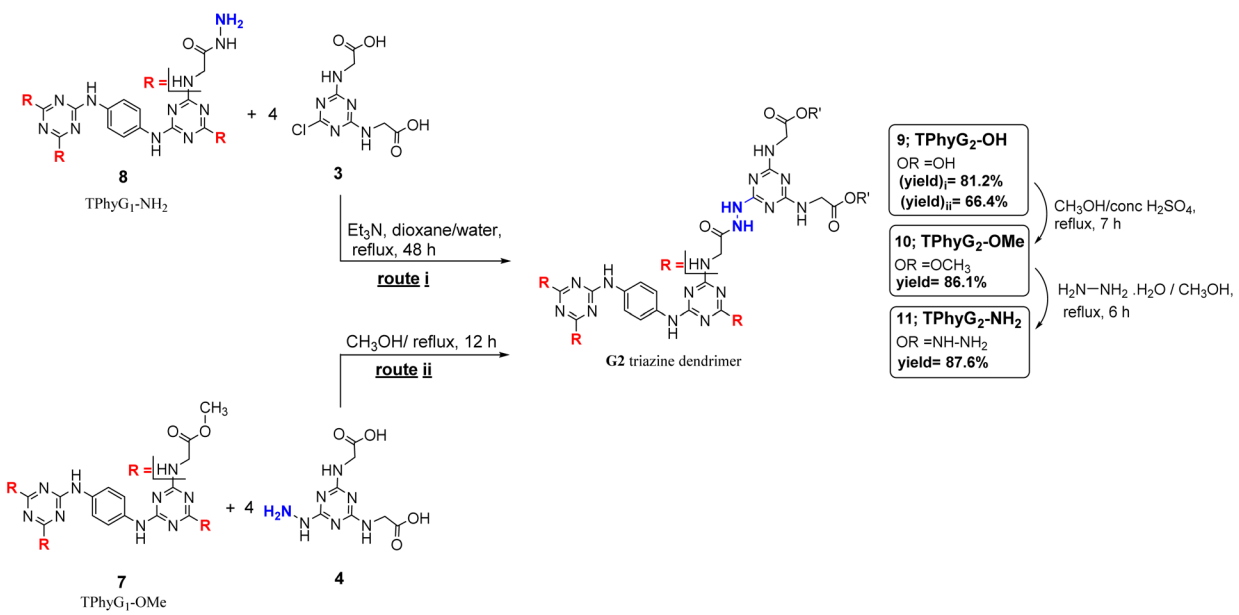

Scheme 3 Synthesis of G2 triazine dendrimers TPhyG$_2$-OH **9**, TPhyG$_2$-OMe **10** and TPhyG$_2$-NH$_2$ **11**.

terminated TPhyG$_2$-OH **9** in methanol to give TPhyG$_2$-OMe **10**, which was later reacted with hydrazine hydrate to yield the respective hydrazide analogue TPhyG$_2$-NH$_2$ **11**. These analogues will be employed later to construct the third generation of our designed architecture. These transformations can be traced in the IR, ^{1}H-NMR and ^{13}C-NMR spectral data of **9**, **10** and **11** where the same manner, previously explained with the G1 analogues **6**, **7** and **8**, was identified.

3.1.5. Synthesis of 3rd generation dendrimers. The third generation was constructed through the same previously explained methods, either by reacting the nucleophilic NH$_2$ groups of the hydrazide G2 analogue **11** with the chlorine atom of repeating unit **3** (8 equivalents) (Scheme 4, route i) or *via* acyl nucleophilic substitution of ester groups in the respective G2 analogue **10** by the hydrazide functionality in repeating unit **4** (8 equivalents) (Scheme 4, route ii). The former method repeatedly proves to be more successful, giving the desired G3 dendrimer TPhyG$_3$-OH **12** in a very good yield (~90%), which is yet again higher than that obtained with the latter pathway by 16%. Moreover, the G3 ester terminated analogue **13** and its corresponding hydrazide **14** were prepared in very good yields following the same transformations explained before with their respective G2 analogues. Investigation of the spectra of any of the reported G3 analogues confirms the growth of the dendrimer into the third generation indicated by the increase in integration of the characteristic peaks corresponding to glycine CH$_2$ protons as a result of incorporating 8 new repeating units (16 terminal groups) in the obtained G3 dendrimer.

3.1.7. Synthesis of 4th generation dendrimers. For the final G4 triazine dendrimer TPhyG$_4$-OH **15**, only the more effective method was employed. The G3 dendrimer **14** possessing 16 nucleophilic hydrazide end groups was allowed to react with 16 equivalents of the monochlorinated triazine repeating unit **3** (Scheme 5). The nucleophilic substitution resulted in TPhyG$_4$-OH **15** in ~ 87% yield which is a relatively very satisfying yield for such macromolecule with 32 carboxylic end groups. The carboxyl termini were left unaltered as they will be exploited later in coupling of quercetin, lactobionic acid and polyethylene glycol to the dendritic structure. Analysis of the ^{1}H-NMR spectrum of **15** in DMSO-d_6 revealed a multiplet peak corresponding to 120 α-methylene protons arising from 64 external and 56 internal glycine residues. While the integration of the aromatic peak corresponds to the four protons of the phenylene core. Therefore, the successful growth of the dendritic structure into a fourth generation was confirmed.

3.1.8. Coupling of G3 and G4 dendrimers with quercetin, lactobionic acid and subsequent PEGylation. PEGylated lactobionic acid-targeted quercetin-G3(G4) dendrimer conjugates (**18** and **21**) were obtained in three stages involving activation/coupling steps (Scheme 6). In the first stage, the free acid-terminated dendrimers TPhyG$_{3(4)}$-OH **12** (**15**) were pre-activated and coupled with quercetin (QUR) following the coupling conditions that involve *N*,*N*′-diisopropylcarbodiimide (DIC) as a coupling agent and oxyma as an additive.[60,81–83] Then the formed dendrimer-quercetin conjugates (TPhyG$_{3(4)}$-OH)-QUR **16** (**19**) were purified by dialysis and the concentration of unconjugated quercetin in dialysate was determined by HPLC. From the ^{1}H-NMR spectra of **16** and **19**, it can be deduced that three quercetin molecules were coupled to **16**, while the more branched G4 analogue **19** was able to conjugate five molecules of quercetin. This was concluded by interpreting the integration of signals characteristic to the aromatic protons of quercetin, in addition to its OH signals, as each coupled quercetin molecule have 5 aromatic protons and 4 free OH's. New 15 aromatic protons and 12 OH protons were detected in the ^{1}H-NMR spectrum of **16** at δ 6.13–7.85 and 8.70–9.02 ppm, respectively,

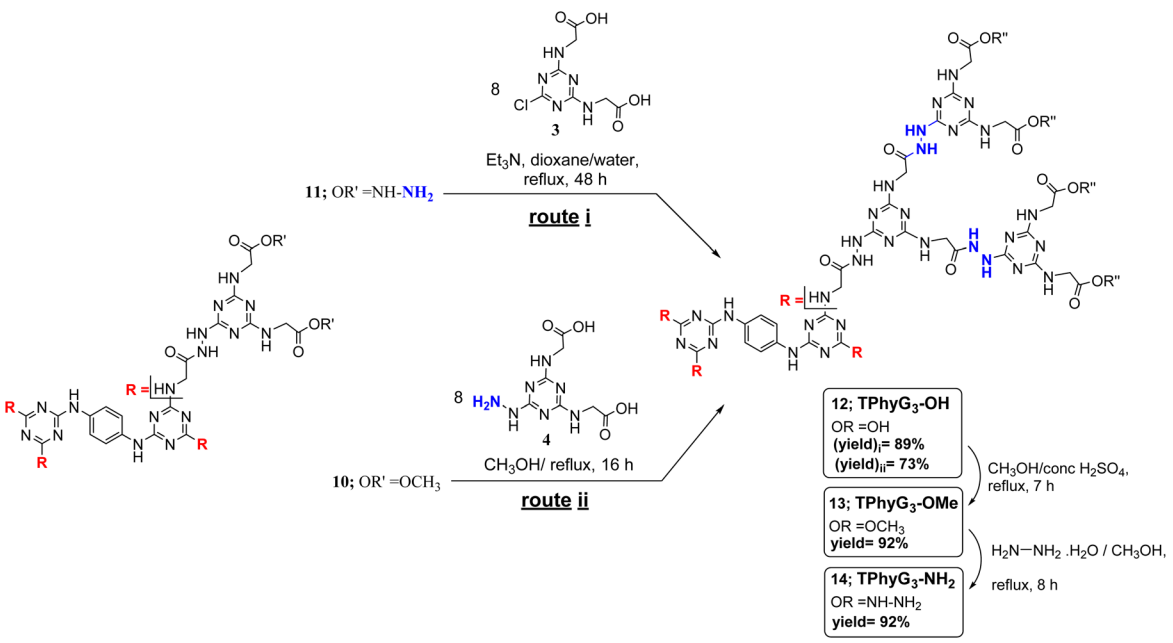

Scheme 4 Synthesis of G3 triazine dendrimers TPhyG$_3$-OH **12**, TPhyG$_3$-OMe **13** and TPhyG$_3$-NH$_2$ **14**.

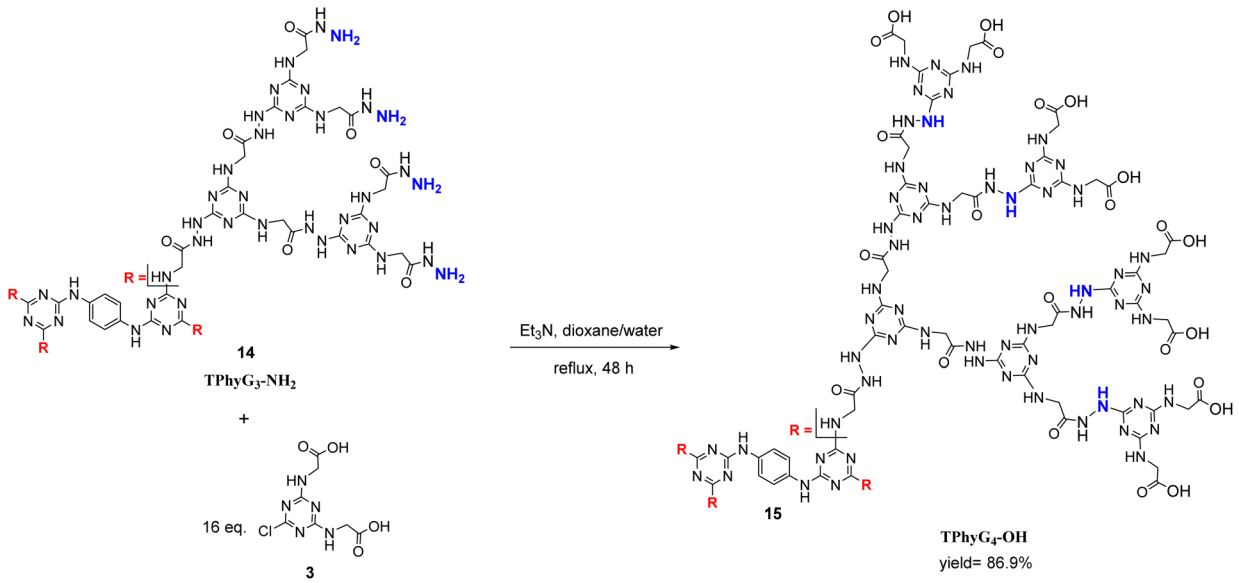

Scheme 5 Synthesis of G4 triazine dendrimer TPhyG$_4$-OH **15**.

confirming the conjugation of 3 quercetin molecules into the G3 structure. On the other hand, the ^{1}H-NMR spectrum of **19** revealed the presence of new 25 aromatic protons at δ 6.16–7.86 ppm as well as new 20 hydroxyl protons at δ 9.21–12.57 ppm, proving the coupling of five quercetin molecules with the carboxyl termini of the G4 dendrimer. The second stage involves conjugation of the acquired quercetin coupled dendrimers **16** (**19**) with lactobionic acid (LA) as targeting ligand to

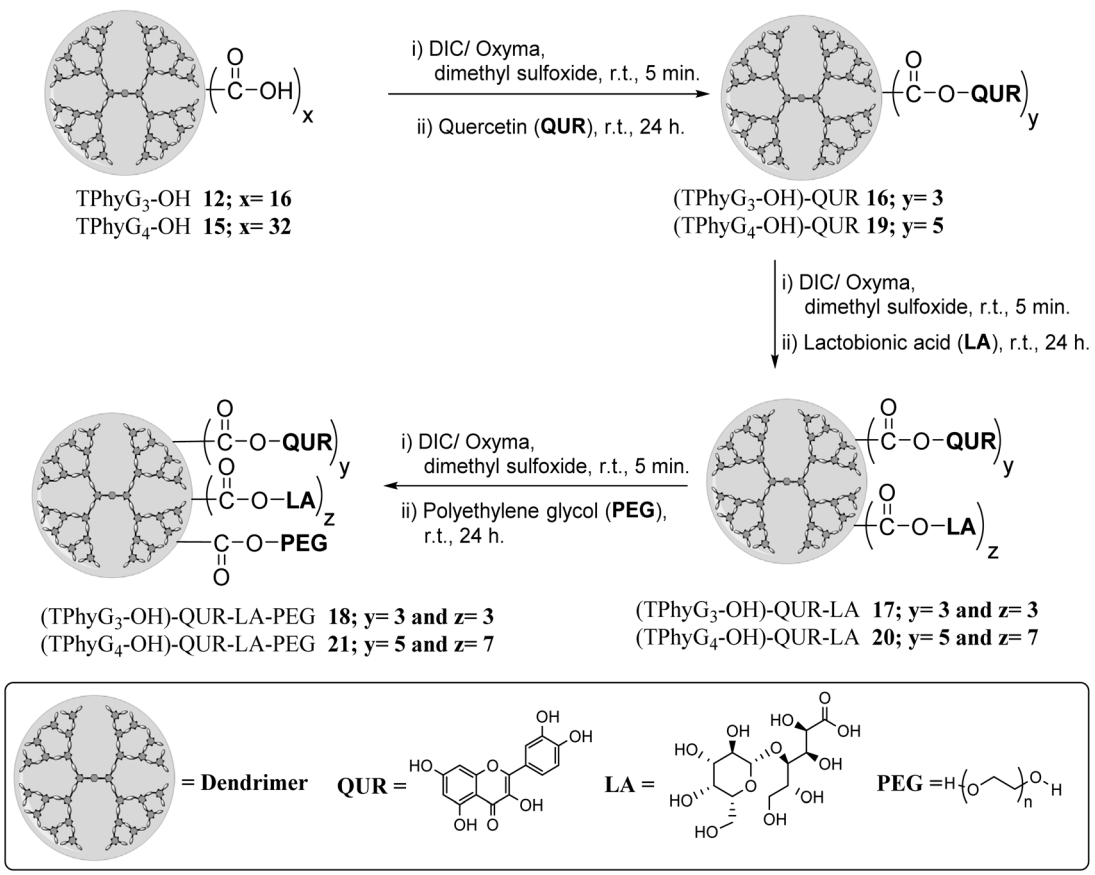

Scheme 6 Synthesis of PEGylated lactobionic acid-targeted Quercetin-dendrimer conjugates **18**–**21**.

Table 1 Physicochemical characterization of Quercetin-dendrimer conjugates **16–21**: drug content, particle size (PS), polydispersity index (PDI) and zeta potential

Nanoparticles	Dendrimer (mg)	Quercetin (mg)	Particle size (nm)	PDI	Zeta potential (mV)
($TPhyG_3$-OH)-QUR **16**	50	12.68 (**2.87 equiv.**)	258.7	0.723	−52.7
($TPhyG_3$-OH)-QUR-LA **17**	50	10.21 (**2.31 equiv.**)	196.3	0.655	−56.1
($TPhyG_3$-OH)-QUR-LA-PEG **18**	50	14.58 (**3.30 equiv.**)	**186.7**	**0.345**	**−38.9**
($TPhyG_4$-OH)-QUR **19**	50	9.78 (**4.7 equiv.**)	469.0	0.663	−55.1
($TPhyG_4$-OH)-QUR-LA **20**	50	12.04 (**5.8 equiv.**)	313.7	0.656	−50.3
($TPhyG_4$-OH)-QUR-LA-PEG **21**	50	11.21 (**5.38 equiv.**)	**174.9**	**0.249**	**−33.8**

produce ($TPhyG_{3(4)}$-OH)-QUR-LA **17** (**20**) using the same adapted DIC/oxyma approach followed by dialysis work-up. Three molecules of lactobionic acid were detected in the ^{1}H-NMR spectrum of **17**, indicated by the presence of a multiplet peak at 5.12–5.15 ppm corresponding to the three lactobionic anomeric protons and another one at 11.20–11.34 ppm arising from the three lactobionic carboxylic OH groups which further confirms the conjugation of 3 LA molecules to the starting G3 conjugate **16**. Tracing the integration of the same signals of the LA residue in the ^{1}H-NMR spectrum of **20** revealed that 7 molecules of lactobionic acid were successfully coupled to the G4 dendrimer conjugate **19**. Thus, the presence of more free acid end groups in **19** allowed for the coupling of four more LA molecules compared to its respective G3 analogue **16**. The third and final stage is PEGylation of the targeted conjugates **17** (**20**), obtained in stage 2, through their activation with DIC/Oxyma followed by addition of polyethylene glycol (PEG) which afforded the PEGylated lactobionic acid targeted dendrimer-quercetin conjugates ($TPhyG_{3(4)}$-OH)-QUR-LA-PEG **18** (**21**). The original G3 carboxyl-terminated dendrimer **12** had **16** acid end groups, three of them were coupled with QUR and another three were conjugated to LA, leaving behind 10 free COOH terminal groups. The ^{1}H-NMR spectrum of ($TPhyG_3$-OH)-QUR-LA-PEG **18** indicates the presence of only 9 unconjugated OH end groups as a result of coupling of one carboxyl end group upon PEGylation. On the other hand, the free acid terminated G4 dendrimer had 32 end groups, 5 of them conjugated with quercetin and 7 with lactobioinic acid, therefore 20 carboxyl end groups remained unconjugated in the resulting conjugate **17**. The ^{1}H-NMR spectrum of ($TPhyG_4$-OH)-QUR-LA-PEG **21** depicts the presence of 19 free OH end groups, indicating the PEGylation of one COOH. Moreover, the ethylene glycol residue in the final structure is clearly evident in the spectra of both **18** and **21**, where the characteristic PEG (–O–CH_2CH_2) protons appeared as a multiplet peak at ∼ 3.40–3.54 ppm, and the free PEG hydroxyl proton appeared as another multiplet at ∼ 4.54–4.74 ppm.

3.1.9. Physicochemical characterization of quercetin-dendrimer conjugates. An HPLC calibration method was developed to quantify the amount of unconjugated quercetin remaining in the dialysate after each dialysis of the QUR-conjugates **16–21** (for chromatographic conditions see S19 in ESI†). The drug content in QUR-coupled dendrimers **16–21** reflected by the amount of conjugated QUR was determined indirectly by subtracting the unreacted QUR from the initial QUR amount (Table 1). HPLC analysis revealed that the quercetin content was ∼ 3 equivalents in the G3 conjugates **16–18** and ∼ 5 equivalents in the G4 conjugates **19–21**, consistent with the ^{1}H-NMR findings explained before. Particle size, polydispersity index (PDI) and zeta potential of the QUR-conjugates **16–21** nanoparticles are reported in Fig. 2, 3 and Table 1. Particle size distribution of the G3 triazine dendrimer conjugates **16–18** are 258.7, 196.3 and 186.7 nm respectively (Table 1 and Fig. 2a–c), and their zeta potential in the range of (−38.9) to (−56.1) mV (Table 1 and Fig. 2a′–c′). Particle size of the larger and more branched G4 conjugates **19–21** are 469.0, 313.7 and 174.9 nm (Table 1 and Fig. 3a–c), and the zeta potential of their dispersed particles are in the range of (−33.8)–(−55.1) mV (Table 1 and Fig. 3a′–c′).

PEG coating is known to enhance the biophysical and chemical properties of nanoparticles.[84] Conjugation of PEG to the dendrimers end groups forms a protective layer around the nanoparticle which increases the steric distance between them and increases hydrophilicity by forming hydrogen bonds with the solvent.[85] Thus, it limits aggregation of particles, resulting in a smaller particle size distribution and smaller polydispersity index (PDI) as it can be seen with the PEGylated conjugates **18** and **21** compared to their respective precursors. Zeta potential, which reflects the degree of electrostatic repulsion between adjacent charged particles, also decreases upon PEGylation. All the tested dendrimer conjugates (16–21) exhibited negative zeta potential, which indicates the stability of the dispersed nanoparticles.

3.1.10. Morphological analysis (FE-TEM). The Field Emission Transmission Electron Microscopy (FE-TEM) images of the PEGylated conjugates ($TPhyG_3$-OH)-QUR-LA-PEG **18** and ($TPhyG_4$-OH)-QUR-LA-PEG **21** nanoparticles revealed the presence of spherical to oval particles in the nano size range of 154.28–165.04 and 83.56–164.82, respectively (Fig. 4). Which is relatively smaller than that measured by the zetasizer through dynamic light scattering DLS (**18** : 186.7 nm, **21** : 174.9 nm), this could be a result of shrinkage due to dehydration of nanoparticles during preparation for TEM analysis.[86–88]

3.2. Biology

3.2.1. Cytotoxicity screening on normal human cells. Cytotoxicity of the free dendrimers as well as their conjugated analogues have been assigned by recording their EC_{100} values (μM) for the growth of normal human cells (Wi-38) (Table 2).

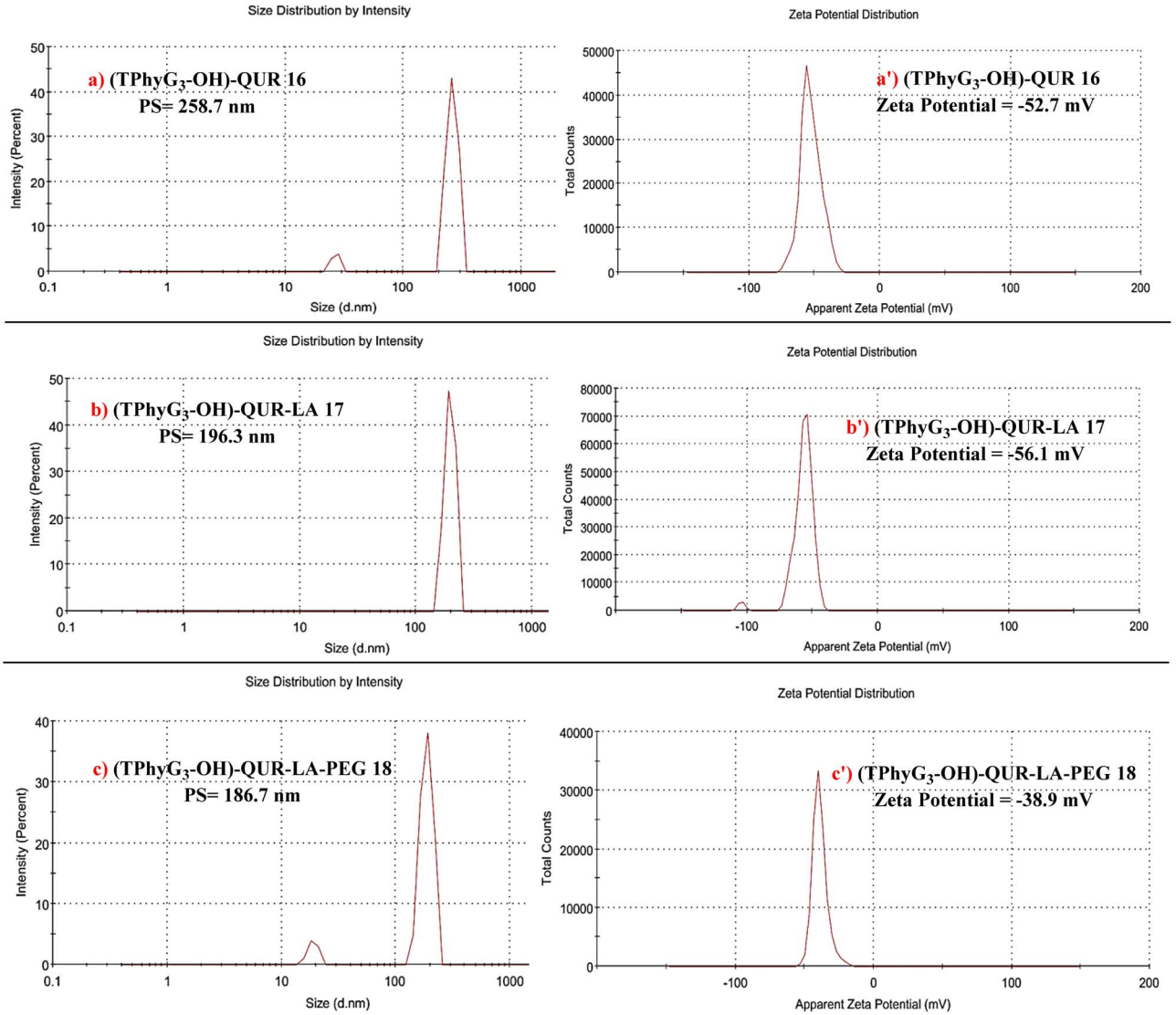

Fig. 2 Particle size distributions (a–c) and zeta potentials (a′–c′) of G3 conjugates **16–18**.

The third-generation dendrimer with free carboxyl end groups ($TPhyG_3$-OH) **12** showed the highest EC_{100} value (147.29 μM) compared to the evaluated dendrimers as well as QUR (EC_{100} = 70.57 μM). Its fourth-generation analogue ($TPhyG_4$-OH) **15** recorded a relatively high EC_{100} value (104.02 μM) as well. As indicated by the higher EC_{100} values, all the quercetin-coupled dendrimers: ($TPhyG_3$-OH)-QUR **16**, ($TPhyG_3$-OH)-QUR-LA **17**, ($TPhyG_3$-OH)-QUR-LA-PEG **18**, ($TPhyG_4$-OH)-QUR **19**, ($TPhyG_4$-OH)-QUR-LA **20**, and ($TPhyG_4$-OH)-QUR-LA-PEG **21** showed better safety profiles compared to QUR. The PEGylated third and fourth generation dendrimers coupled with QUR and LA, ($TPhyG_3$-OH)-QUR-LA-PEG **18** and ($TPhyG_4$-OH)-QUR-LA-PEG **21** showed superior safety profiles compared to their precursors with EC_{100} values of 134.35 μM and 90.64 μM, respectively.

3.2.2. *In vitro* matrix metalloproteinase-2/9 inhibition activity. The intrinsic MMP-2/9 inhibitory potential of the dendritic carriers was evaluated *in vitro* with reference to *N*-isobutyl-*N*-(4-methoxyphenylsulfonyl)glycyl hydroxamic acid (**NNGH**), a broad spectrum hydroxamate-based inhibitor (Table 3). Results revealed that the **G3** dendrimer exhibited an exceptional potency against MMP-9 with an IC_{50} of 0.074 μM being superior to **G4** (IC_{50} = 0.174 μM) and the reference inhibitor (IC_{50} = 0.277 μM). However, the two studied dendrimers were nearly equipotent as MMP-2 inhibitors (IC_{50} = 0.35 μM) and comparable to NNGH. Interestingly, **G3** dendrimer is more selective towards MMP-9 over MMP-2 (SI = 4.77 folds).

3.2.3. *In vitro* cytotoxicity evaluation of the dendrimers and their conjugates on human breast cancer cell line (MCF-7 cells) and hepatocellular carcinoma (HepG-2). The potential cytotoxic activities of all the studied dendrimers were assayed against MCF-7 and HepG-2 cells (Table 4). Apart from the third-generation carboxyl-terminated dendrimer ($TPhyG_3$-OH) **12**, all the other studied dendrimeric conjugates were superior to free QUR. Notably, the fourth-generation conjugates exhibited higher cytotoxic activities against MCF-7 cells than their respective third generation precursors. The same trend can be

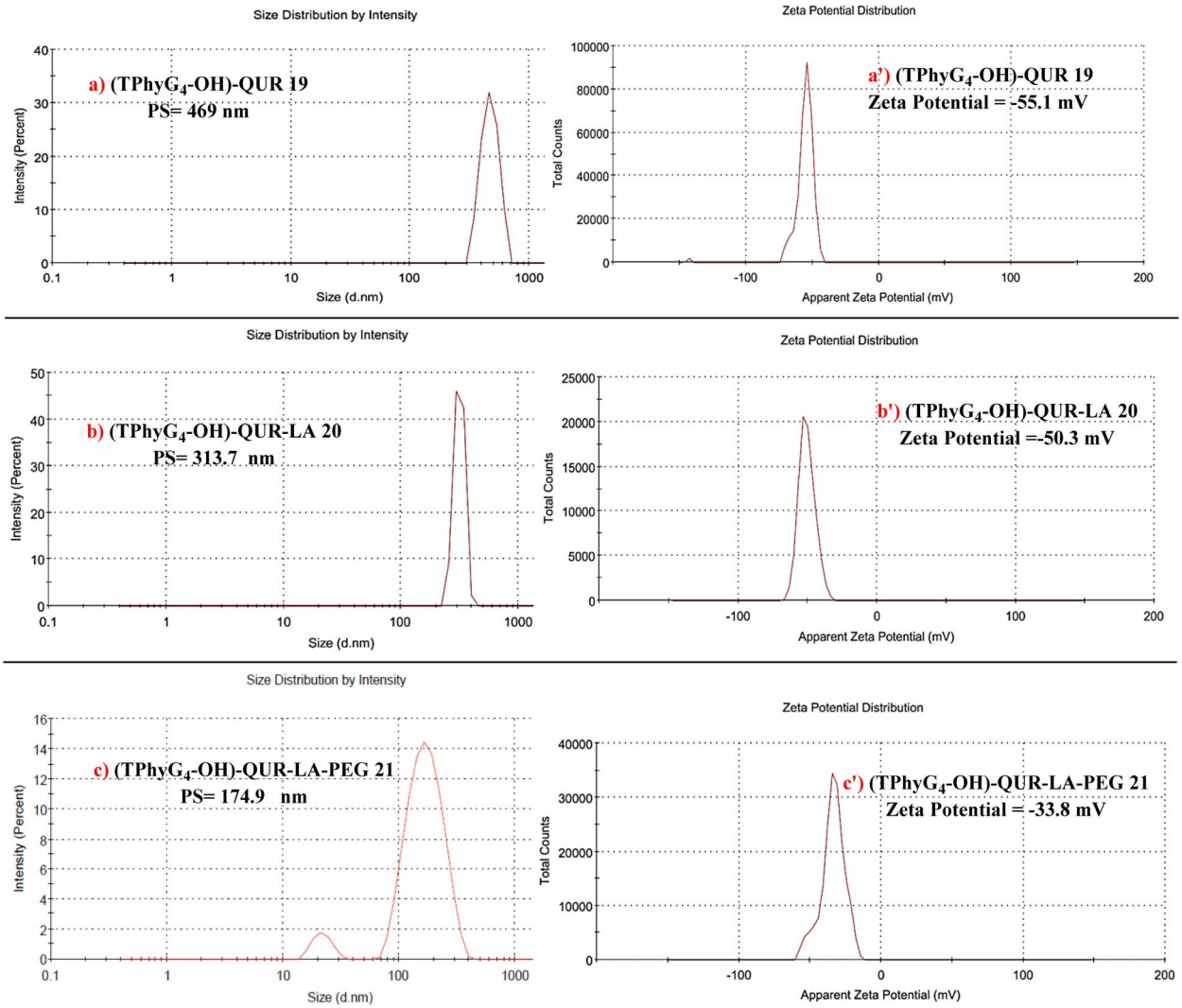

Fig. 3 Particle size distributions (a–c) and zeta potentials (a′–c′) of G4 conjugates **19–21**.

noticed with HepG-2 cells, except for (TPhyG$_3$-OH)-QUR-LA **17** which exhibit a lower IC$_{50}$ (~13 μM) than its respective G4 analogue (TPhyG$_4$-OH)-QUR-LA **20** (IC$_{50}$ = 17.5 μM). Conjugation of lactobionic acid in (TPhyG$_3$-OH)-QUR-LA **17** and (TPhyG$_4$-OH)-QUR-LA **20** resulted in a slight enhancement in the anticancer activity against MCF-7 cell line relative to their corresponding precursors. On the other hand, a remarkable increase in activity against HepG-2 cells was recorded upon introducing lactobionic acid to the dendrimeric scaffold. The PEGylated dendrimers (TPhyG$_3$-OH)-QUR-LA-PEG **18** and (TPhyG$_4$-OH)-QUR-LA-PEG **21** were the most potent against both MCF-7 and HepG-2 cells, with a significantly lower IC$_{50}$ values compared to their non-PEGylated analogues and free QUR. An outstanding potency against HepG-2 cells was observed upon PEGylation of the dendrimers as indicated by their single digit μM IC$_{50}$ values, especially (TPhyG$_4$-OH)-QUR-LA-PEG **21** that surpassed its **G3**-analogue (TPhyG$_3$-OH)-QUR-LA-PEG **18** against MCF-7 and HepG-2 cells. This was expected since the **G4** dendrimer was able to conjugate two more drug (**QUR**) molecules and four more targeting agent (**LA**) molecules (see Scheme 6). Since the **G4** dendrimer (32 terminal groups) was conjugated to 5 molecules of QUR and 7 of LA, while its **G3** analogue (16 terminal groups) coupled with 3 molecules of QUR and 3 of LA. The notable cytotoxic activities of (TPhyG$_3$-OH)-QUR-LA-PEG **18** and (TPhyG$_4$-OH)-QUR-LA-PEG **21** were also inspected by the observable morphological collapse in the treated MCF-7 and HepG-2 cells (Fig. 5).

The dendrimers' selectivity was assessed towards MCF-7 and HepG- 2 cancer cells *versus* normal Wi-38 cells for prioritizing them.[89] Herein, all the tested dendrimers and conjugates showed notably high selectivity index values (SI = 7.610–91.797) reflecting their safety. All dendrimers were much more selective than QUR (SI ~ 8.5) except for (TPhyG$_4$-OH)-QUR-LA **20** against MCF-7 (SI = 7.610). Interestingly, the most potent dendrimeric conjugates (TPhyG$_3$-OH)-QUR-LA-PEG **18** and (TPhyG$_4$-OH)-QUR-LA-PEG **21** recorded the highest selectivity values among the evaluated series against the two screened cancer cell lines. Obviously, the **G4** free dendrimer showed higher selectivity than

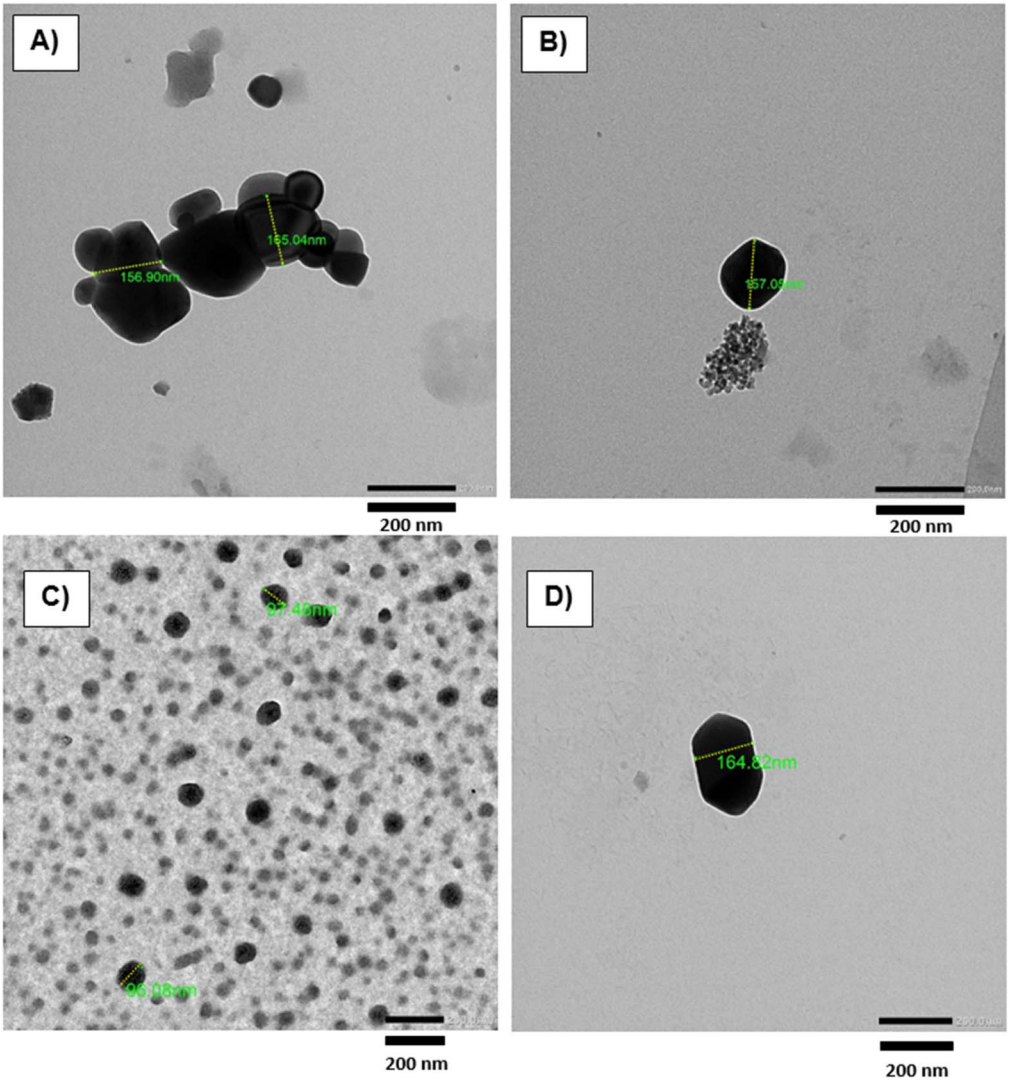

Fig. 4 TEM images showing dendrimers **18** and **21** nanoparticles morphology. (A and B) TEM of G3 conjugate (TPhyG$_3$-OH)-QUR-LA-PEG **18**. (C and D) TEM of G4 conjugate (TPhyG$_4$-OH)-QUR-LA-PEG **21**.

Table 2 Cytotoxicity of the tested dendrimers and their conjugates on normal human fibroblasts (Wi-38)

Dendrimer code	EC_{100} [μM][a]
(TPhyG$_3$-OH) **12**	147.29 ± 0.991
(TPhyG$_3$-OH)-QUR **16**	87.95 ± 1.163
(TPhyG$_3$-OH)-QUR-LA **17**	84.36 ± 0.050
(TPhyG$_3$-OH)-QUR-LA-PEG **18**	**134.35 ± 1.86**
(TPhyG$_4$-OH) **15**	104.02 ± 3.689
(TPhyG$_4$-OH)-QUR **19**	78.44 ± 0.502
(TPhyG$_4$-OH)-QUR-LA **20**	82.85 ± 0.742
(TPhyG$_4$-OH)-QUR-LA-PEG **21**	**90.64 ± 1.614**
Qur	70.57 ± 0.950

[a] Values are presented as mean ± SEM.

its **G3.** Their QUR conjugates (TPhyG$_4$-OH)-QUR **19** and TPhyG$_3$-OH)-QUR **16** exhibited nearly similar selectivity. Interestingly, LA and PEGylation led to enhanced selectivity relative to all precursors.

Table 3 Matrix metalloproteinase-2/9 inhibitory activities of the free dendrimers **12** and **15**

Dendrimer code	MMP-2 IC_{50} (μM)	MMP-9 IC_{50} (μM)	MMP-2/MMP-9 selectivity
(TPhyG$_3$-OH) 12	0.353	0.074	4.77
(TPhyG$_4$-OH) 15	0.359	0.174	2.06
NNGH	0.299	0.277	1.08

3.2.4. Flow cytometric analysis of apoptosis. As depicted in Table 5 and Fig. 6, all the QUR-conjugated dendrimers surpassed the apoptotic induction potential of free QUR in both MCF-7 and HepG-2 cancer cells recording more than 50% apoptotic cell population. Coupling of LA to the carboxyl-terminated dendrimers notably improved the apoptotic induction performance against MCF-7 and HepG-2 cell populations, by >16%, ∼ 5% in (TPhyG$_3$-OH)-QUR-LA **17** and >20%, ∼ 7% in

Table 4 Cytotoxic activities of the dendrimers and their conjugates on MCF-7 and HepG-2 cells

	Wi-38	MCF-7		HepG-2	
Dendrimer code	IC_{50} [μM][a]	IC_{50} [μM][a]	SI	IC_{50} [μM][a]	SI
($TPhyG_3$-OH) **12**	632.83 ± 20.4	36.780 ± 0.180***	17.205	43.947 ± 0.385***	14.399
($TPhyG_3$-OH)-QUR **16**	310.59 ± 15.4	29.316 ± 0.388***	10.594	29.090 ± 1.516***	10.676
($TPhyG_3$-OH)-QUR-LA **17**	367.71 ± 12.5	28.121 ± 0.017***	13.075	13.036 ± 1.025***	28.207
($TPhyG_3$-OH)-QUR-LA-PEG 18	**487.08 ± 4.04**	**18.809 ± 0.260**	**25.896**	**5.306 ± 0.371**	**91.797**
($TPhyG_4$-OH) **15**	556.79 ± 21.8	24.859 ± 0.527**	22.397	23.771 ± 1.593**	23.423
($TPhyG_4$-OH)-QUR **19**	264.78 ± 13.7	26.147 ± 0.167***	10.126	21.932 ± 0.456***	12.072
($TPhyG_4$-OH)-QUR-LA **20**	195.29 ± 16.6	25.660 ± 0.001***	7.610	17.554 ± 1.134***	11.125
($TPhyG_4$-OH)-QUR-LA-PEG 21	**341.51 ± 9.19**	**12.690 ± 0.226**	**26.911**	**4.137 ± 0.314**	**82.550**
Qur	294.27 ± 12.6	35.288 ± 0.475***	8.339	34.323 ± 0.128***	8.573

[a] Values are presented as mean ± SEM. ($TPhyG_3$-OH)-QUR-LA-PEG **18** was compared with ($TPhyG_3$-OH) **12**, ($TPhyG_3$-OH)-QUR **16**, ($TPhyG_3$-OH)-QUR-LA **17**, ($TPhyG_3$-OH)-QUR-LA-PEG **18** and Qur while ($TPhyG_4$-OH)-QUR-LA-PEG **21** was compared with ($TPhyG_4$-OH) **15** and ($TPhyG_4$-OH)-QUR **19**, ($TPhyG_4$-OH)-QUR-LA **20**, ($TPhyG_4$-OH)-QUR-LA-PEG **21** and Qur. These comparisons were considered significantly different at $p < 0.05$*, $p < 0.005$**, $p < 0.0005$***.

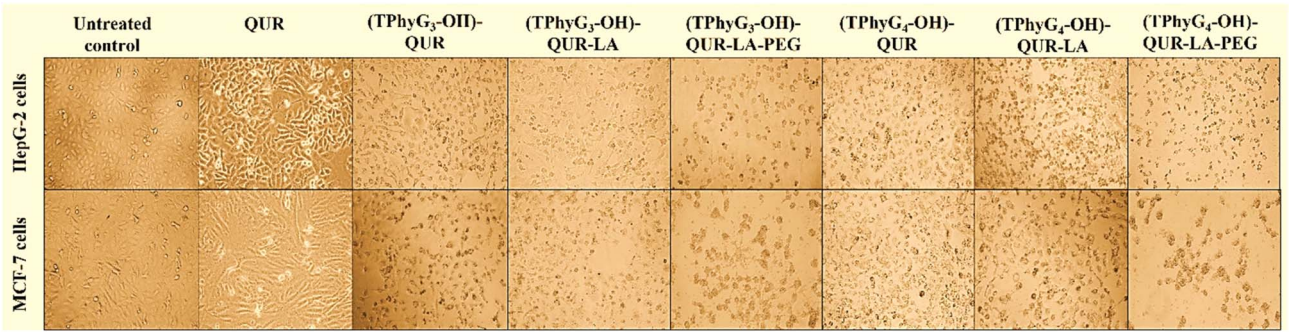

Fig. 5 Morphological alteration of the dendrimers-treated MCF-7 and HepG-2 cells in comparison with the QUR-treated cancer cells and the untreated control cells.

($TPhyG_4$-OH)-QUR-LA **20** treated cells, respectively. Further PEGylation led to increased apoptotic population compared to their respective precursors in both treated cancer cells.

Table 5 The total percentage of the apoptotic cell population in dendrimer-treated MCF-7 and HepG-2 cell lines

	Total % of the apoptotic population[a]	
Dendrimer code	**MCF-7**	**HepG-2**
($TPhyG_3$-OH)-QUR **16**	53.39 ± 2.27**	50.29 ± 1.065*
($TPhyG_3$-OH)-QUR-LA **17**	69.63 ± 1.09	55.22 ±1.14
($TPhyG_3$-OH)-QUR-LA-PEG 18	**74.25** ± 1.62[b]	**55.00** ± 1.465[b]
($TPhyG_4$-OH)-QUR **19**	52.81 ± 4.23*	51.84 ± 1.36**
($TPhyG_4$-OH)-QUR-LA **20**	73.24 ± 1.48	58.94 ± 1.95*
($TPhyG_4$-OH)-QUR-LA-PEG 21	**74.43** ± 2.39[b]	**66.82** ± 0.395[b]
Untreated control	0.530 ± 0.03***	1.995 ± 0.025***
Qur	47.00 ± 1.83***	24.20 ± 0.895**

[a] Values are presented as mean ± SEM. [b] Highest percentage of apoptotic population compared to their precursors, untreated control and free **Qur**. ($TPhyG_3$-OH)-QUR-LA-PEG **18** was compared with ($TPhyG_3$-OH)-QUR **16**, ($TPhyG_3$-OH)-QUR-LA **17**, and Qur while ($TPhyG_4$-OH)-QUR-LA-PEG **21** was compared with ($TPhyG_4$-OH)-QUR **19**, ($TPhyG_4$-OH)-QUR-LA **20**, and Qur. These comparisons were considered significantly different at $p < 0.05$*, $p < 0.005$**, $p < 0.0005$***.

However, this effect is more evident with **G3** conjugates-treated MCF-7 cells, and **G4** conjugates-treated HepG-2 cells. Both third and fourth generation PEGylated dendrimers ($TPhyG_3$-OH)-QUR-LA-PEG **18** and ($TPhyG_4$-OH)-QUR-LA-PEG **21** exhibited similar potency against MCF-7, inducing apoptosis in more than 74% of the treated cancer cells. While a difference of ∼ 12% in apoptotic population was recorded between the two dendrimers in case of HepG-2 cells.

3.2.5. VEGF downregulation. Based on the interplay between MMP-9 and VEGF,[90] the regulatory potential of the studied dendrimers on VEGF expression levels in both MCF-7 and HepG-2 cancer cells was investigated utilizing quantitative real-time PCR analysis (Table 6). Herein, the observed results of the studied dendrimers were directly correlated to their cytotoxic profiles (Table 4). Similar trends can be tracked where generally all the studied dendrimers surpassed the downregulation potential of free QUR, with **G4** conjugates at the top of the list. Incorporation of lactobionic acid as a targeted ligand into the dendritic architecture allowed for enhanced downregulation potential and even further improvement was achieved upon PEGylation. Among all the studied dendrimers, the PEGylated conjugates, ($TPhyG_3$-OH)-QUR-LA-PEG **18** and ($TPhyG_4$-OH)-QUR-LA-PEG **21** exhibited the maximum potential

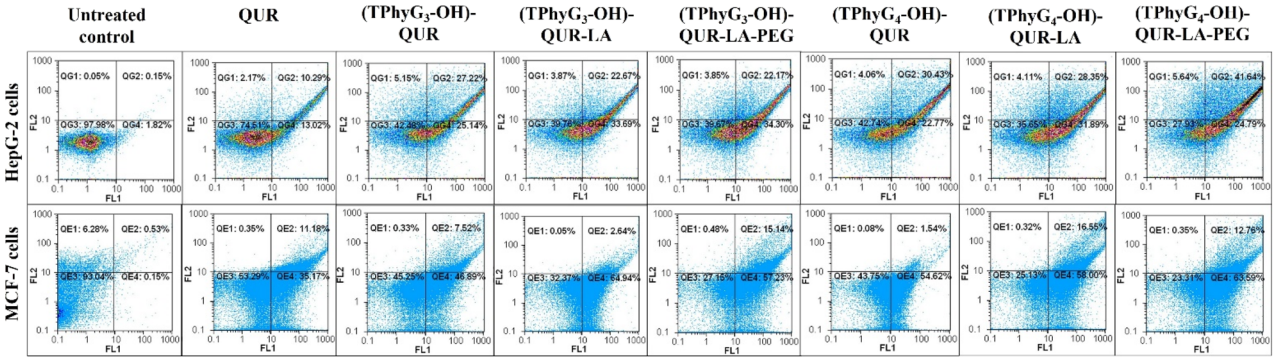

Fig. 6 Flow charts of annexin-PI analysis of the dendrimers-treated MCF-7 and HepG-2 cells in comparison with the QUR-treated cancer cells and the untreated control cells.

Table 6 Relative fold change in gene expression levels of VEGF in dendrimer-treated MCF-7 and HepG-2 cells

	VEGF relative fold change[a]	
Dendrimer code	(MCF-7)[b]	(HepG-2)[b]
(TPhyG$_3$-OH)-QUR **16**	0.597 ± 0.009***	0.635 ± 0.068***
(TPhyG$_3$-OH)-QUR-LA **17**	0.318 ± 0.002***	0.238 ± 0.019***
(TPhyG$_3$-OH)-QUR-LA-PEG 18	**0.282** ±0.018***	**0.181** ± 0.017***
(TPhyG$_4$-OH)-QUR **19**	0.310 ± 0.006***	0.530 ± 0.069***
(TPhyG$_4$-OH)-QUR-LA **20**	0.146 ± 0.010	0.193 ± 0.009
(TPhyG$_4$-OH)-QUR-LA-PEG 21	**0.112** ± 0.011	**0.160** ± 0.013
Qur	0.683 ± 0.029***	0.708 ± 0.012***

[a] Compared to the gene expression levels of VEGF in untreated cells. [b] Values are presented as mean ± SEM. (TPhyG$_4$-OH)-QUR-LA-PEG 21 was compared with other compounds. These comparisons were considered significantly different at $p < 0.05$*, $p < 0.005$**, $p < 0.0005$***.

for suppressing VEGF gene expression in both treated cancer cells.

3.2.6. Structure-activity relationship. The conducted biological evaluation showed that all the QUR-coupled dendrimers demonstrated higher cytotoxic potency against MCF-7 and HepG-2 cancer cells compared to free QUR while being highly tolerated by normal human cells. Results (Tables 2 and 4) revealed clear correlation between the type of conjugated decoration on the peripheries of the designed dendrimer and their cytotoxicity. Conjugation of LA as a targeting ligand to the carboxyl terminated dendrimer rendered it more cytotoxic towards both treated cancer cells, with the effect being more prominent on HepG-2 cells. Further PEGylation of the dendritic termini lead to a notable increase in potency against both MCF-7 and HepG-2 cells together with promising selectivity towards cancer cells over normal cells. Incorporation of LA and polyethylene glycol into the dendritic structure conferred high apoptosis induction potential and VEGF suppression in both MCF-7 and HepG-2 cancer cells. In almost all of the aforementioned evaluations, the fourth-generation dendrimers **G4** displayed a more promising anticancer performance relative to their respective **G3** analogues and free QUR, regarding cytotoxic activities, apoptotic induction potential and VEGF gene expression levels in both examined cancer cells with concentrations that are much below their safe doses (EC_{100}). This may be attributable to the fact that **G4** dendrimer termini carry more molecules of quercetin and lactobionic acid targeting agent compared to the less branched **G3** analogue. The only deviation from this clear trend in potency was noted during assessment of the inhibitory potential of the free acid-terminated dendrimers against MMP-2/9, where both **G3** and **G4** dendrimers displayed similar MMP-2 inhibition activity while **G3** dendrimer were more potent and more selective towards MMP-9 than its **G4** analogue.

3.2.7. Docking studies. The most active dendrimer (TPhyG$_3$-OH) **12** was docked into MMP-9 active site to explore its possible binding mode utilizing MOE 2019.102.[91] The catalytic domain of MMP-9 crystallized with a reverse hydroxamate inhibitor without prodomains and fibronectin was retrieved from the protein data bank (PDB ID: 1GKC)[92] and prepared according to the default structure preparation module of MOE after removing unwanted residues. The optimized MMP-9 domain thus consists of one monomer containing two zinc and three calcium ions. The energy minimized dendrimer was docked into the ligand binding site. Simulations were then conducted applying different fitting protocols for validation. Rigid docking was adopted employing the Triangular matcher algorithm and Alpha HB scoring function for generating the top non-redundant poses of the lowest binding energy conformers. The best docked pose ($\Delta G = -15.37$ kcal mol^{-1}) (Fig. 7) showed that the extended carboxylic acid termini could reach and chelate the active site Zn as roughly expected. The dendrimeric scaffold was observed extended along the catalytic domain interacting with His411 that normally coordinates the active site Zn, the S1′ subpocket Asp185, the backbone Met422 as well as the catalytic domain residues Gly215 and Gly392.

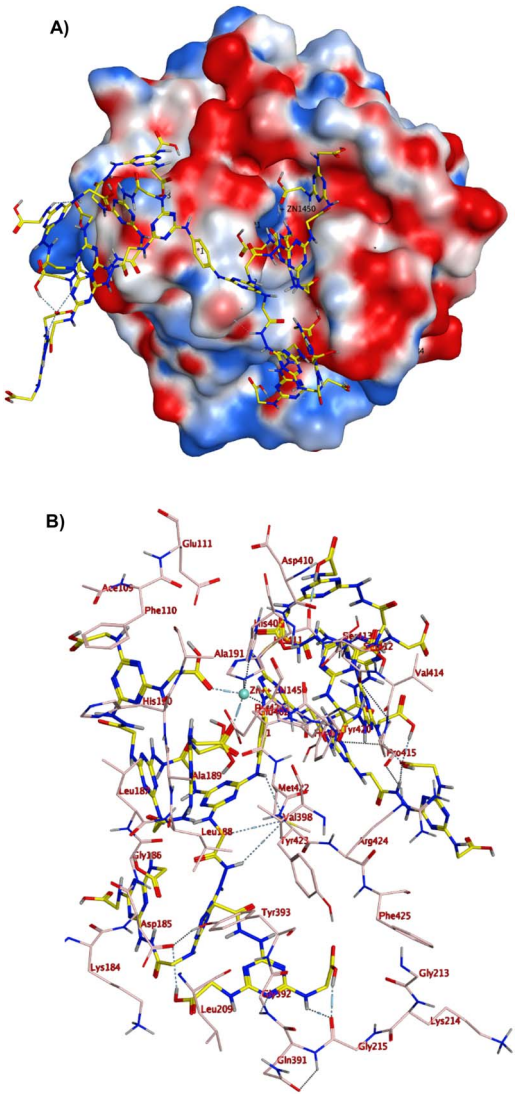

Fig. 7 (A) Molecular surface of MMP-9 catalytic domain showing active site zinc ion and the docked dendrimer **12** (yellow sticks), and (B) 3D binding mode of **12** (yellow sticks) in the catalytic domain of MMP-9 (PDB ID: 1GKC[2]).

4. Conclusions

The current study portrays tailoring new bioactive **G4** *s*-triazine-based dendrimers decorated with carboxylic acids termini as ZBGs to endow MMP inhibitory potential and amenable to tumor targeting and delivery of conjugated therapeutic payloads. Herein, a simple and easily applicable synthetic method was employed, that allowed for the dendrimers to grow smoothly into different generations in very good yield. The **G3** dendrimer exhibited promising potency against MMP-9 (IC_{50} = 0.074 μM) and selectivity towards MMP-9 over MMP-2 (SI = 4.77 folds) surpassing **G4** (IC_{50} = 0.174 μM) and NNGH (IC_{50} = 0.277 μM). The customizable termini of the dendritic platforms were then coupled *via* biodegradable ester linkages to QUR, a natural multitarget MMP-9 inhibitor, and LA, a targeting ligand for both breast and liver cancer. Accordingly, the engineered conjugate could be viewed as a targeted bullet that can efficiently target MMP-9, the tumor microenvironment modulator and metastatic node, in breast and liver cancerous tissues, not only *via* delivering QUR but also *via* direct enzymatic inhibitory potential of the free dendrimers. The cytotoxic activities were also granted *via* combining the apoptotic induction effects of QUR with the therapeutic outcome of MMP inhibition for halting breast cancer and liver metastasis. Finally, the conjugated dendrimers were PEGylated for enhancing their safety and pharmacokinetic profiles. All the QUR-coupled dendrimers displayed an overall superior anticancer performance against MCF-7 and HepG-2 cancer cells compared to free QUR within their safe doses on normal human fibroblasts. Further conjugation of LA followed by PEGylation boosted the anticancer activity against both examined cancer cells; TPhyG$_3$-OH)-QUR-LA-PEG **18** (MCF-7; IC_{50} = 18.80 μM and HepG-2; IC_{50} = 5.30 μM). And (TPhyG$_4$-OH)-QUR-LA-PEG **21** (MCF-7; IC_{50} = 12.69 μM and HepG-2; IC_{50} = 4.13 μM). Flow cytometric analysis of apoptosis showed that (TPhyG$_3$-OH)-QUR-LA-PEG **18** and (TPhyG$_4$-OH)-QUR-LA-PEG **21** induced MCF-7 and HepG-2 cells apoptosis in more than 74%, 55% of the population, respectively. Further studies revealed that the studied dendrimer conjugates down regulated VEGF expression levels, the critical component of liver metastasis. Notably, the more branched fourth generation dendrimer conjugate appear to function better as a carrier compared to its relative third generation analogue. The reported work enriches the emphasis on the role of dendritic scaffolds as promising drug delivery systems that can be customized with designated drugs, targeting ligands, in addition to pharmacophoric features endowed within the structure of the dendrimer itself, all working in harmony to tackle and conquer tumorous tissues.

5. Experimental

All the chemicals and instruments used are mentioned in detail in the ESI.†

5.1. Chemistry

Synthesis and characterization of all the prepared **G$_3$** and **G$_4$** dendrimers are described in detail in the ESI.†

5.1.1. Physicochemical characterizations of the prepared dendrimer drug conjugates. All the prepared G$_3$ and G$_4$ dendrimer-quercetin conjugate nanoparticles were evaluated for their physicochemical characteristics manifested as particle size (PS), polydispersity index (PDI), zeta potential and conjugation efficiency (% CE), for details see ESI (S19).†

5.2. Biology

All cell lines: Wi-38 (CCL-75), MCF-7 (HTB-22) and HepG-2 (HB-8065), were purchased from the American Type Culture Collection (ATCC, USA).

5.2.1. Cytotoxicity evaluation on normal human lung fibroblasts (Wi-38). Cytotoxicity was assigned following MTT assay as detailed in the ESI (see S20).†

5.2.2. *In vitro* matrix metalloproteinase-2/9 inhibitory activity. The dendrimers (TPhyG$_3$-OH) **12** and (TPhyG$_4$-OH) **15** under investigation were evaluated for *in vitro* MMP-2 and MMP-9 inhibitory activities utilizing MMP-2 inhibitor screening assay colorimetric kit (Abcam, Catalog No. ab139446) and MMP-9 Colorimetric Assay Kit for Drug Discovery- AK-410 [a]A BIOMOL® QuantiZyme™ Assay System, following the manufacturers' instructions as detailed in the ESI.† The results were displayed as mean ± standard deviation (SD). Selectivity index (SI) was calculated as IC_{50} (MMP-2)/IC_{50} (MMP-9), (see ESI S21†).

5.2.3. *In vitro* cytotoxicity evaluation on breast cancer cell line (MCF-7 cells) and hepatocellular carcinoma (HepG-2). Anticancer activities of the synthesized dendrimers were evaluated following procedure detailed in the ESI (see ESI S22).†

5.2.4. Flow cytometric analysis of apoptotic effects of the most active and safe compounds. Procedure for flow cytometric analysis of apoptosis for the following dendrimer drug conjugates (TPhyG$_3$-OH)-QUR, (TPhyG$_3$-OH)-QUR-LA, (TPhyG$_3$-OH)-QUR-LA-PEG, (TPhyG$_4$-OH)-QUR, (TPhyG$_4$-OH)-QUR-LA, (TPhyG$_4$-OH)-QUR-LA-PEG) is detailed in the ESI (see S23).†

5.3. Docking

The adopted structure preparation procedure, settings and docking protocol were detailed in the ESI (see S24).†

5.4. Statistical analysis

The data are expressed as mean ± standard error of mean (SEM) and the significant values were considered at $p < 0.05$*. One-way analysis of variance (ANOVA) by Tukey's test used for evaluating the difference between the mean values of the studied treatments. The analysis was done for three measurements using SPSS software version 16.

Data availability

The data supporting this article have been included either in the main text or as part of the ESI.†

Author contributions

Doaa R. Ramadan: methodology, validation, formal analysis, funding acquisition, project administration, writing original draft, review & editing; Heba A. Osman: methodology, investigation; Somaya Aly Madhy: methodology, investigation; M.Teleb: methodology, formal analysis, writing original draft; A.I. Darwish: supervision; M. M. Abu-Serie: methodology, validation, formal analysis; N. S. Haiba: methodology, formal analysis; Sh. N. Khattab: supervision, conceptualization, writing, review & editing; Hosam H. Khalil: formal analysis, supervision, writing original draft, project administration.

Conflicts of interest

There are no conflicts to declare.

Acknowledgements

The authors thank the Science, Technology & Innovation Funding Authority (STDF), Cairo, Egypt, for funding this work through the Basic Sciences Grant (Proposal ID 48085).

Notes and references

1 H. Sung, J. Ferlay, R. L. Siegel, M. Laversanne, I. Soerjomataram, A. Jemal and F. Bray, *Ca-Cancer J. Clin.*, 2021, **71**, 209–249.
2 Female breast cancer surpasses lung as the most commonly diagnosed cancer worldwide, **http://pressroom.cancer.org/GlobalCancerStats2020**).
3 N. S. Rashid, J. M. Grible, C. V. Clevenger and J. C. Harrell, *Clin. Exp. Metastasis*, 2021, **38**, 263–277.
4 Liver Metastasis, **https://www.breastcancer.org/types/metastatic/liver-metastasis**).
5 E. Heer, A. Harper, N. Escandor, H. Sung, V. McCormack and M. M. Fidler-Benaoudia, *Lancet Glob Health*, 2020, **8**, e1027–e1037.
6 S. D. Soysal, A. Tzankov and S. E. Muenst, *Pathobiology*, 2015, **82**, 142–152.
7 W. G. Stetler-Stevenson, S. Aznavoorian and L. A. Liotta, *Annu. Rev. Cell Biol.*, 1993, **9**, 541–573.
8 C. Walker, E. Mojares and A. Del Río Hernández, *Int. J. Mol. Sci.*, 2018, **19**, 3028–3058.
9 K. Kessenbrock, V. Plaks and Z. Werb, *Cell*, 2010, **141**, 52–67.
10 N. A. Bhowmick, E. G. Neilson and H. L. Moses, *Nature*, 2004, **432**, 332–337.
11 A. F. Chambers and L. M. Matrisian, *J. Natl. Cancer Inst.*, 1997, **89**, 1260–1270.
12 R. Kalluri and M. Zeisberg, *Nat. Rev. Cancer*, 2006, **6**, 392–401.
13 J. Cathcart, A. Pulkoski-Gross and J. Cao, *Genes Dis.*, 2015, **2**, 26–34.
14 S. Curran, S. R. Dundas, J. Buxton, M. F. Leeman, R. Ramsay and G. I. Murray, *Clin. Cancer Res.*, 2004, **10**, 8229–8234.
15 M.-A. Forget, R. R. Desrosiers and R. Béliveau, *Can. J. Physiol. Pharmacol.*, 1999, **77**, 465–480.
16 N. Adhikari, A. Mukherjee, A. Saha and T. Jha, *Eur. J. Med. Chem.*, 2017, **129**, 72–109.
17 R. Visse and H. Nagase, *Circ. Res.*, 2003, **92**, 827–839.
18 S. Brown, S. O. Meroueh, R. Fridman and S. Mobashery, *Curr. Top. Med. Chem.*, 2004, **4**, 1227–1238.
19 E. Nuti, T. Tuccinardi and A. Rossello, *Curr. Pharm. Des.*, 2007, **13**, 2087–2100.
20 D. Georgiadis and A. Yiotakis, *Bioorg. Med. Chem.*, 2008, **16**, 8781–8794.
21 B. G. Rao, *Curr. Pharm. Des.*, 2005, **11**, 295–322.
22 L. M. Coussens, B. Fingleton and L. M. Matrisian, *Science*, 2002, **295**, 2387–2392.
23 C. Gialeli, A. D. Theocharis and N. K. Karamanos, *FEBS J.*, 2011, **278**, 16–27.
24 C. M. Overall and O. Kleifeld, *Nat. Rev. Cancer*, 2006, **6**, 227–239.

25 E. Breuer, J. Frant and R. Reich, *Expert Opin. Ther. Pat.*, 2005, **15**, 253–269.
26 M. Whittaker, C. D. Floyd, P. Brown and A. Gearing, *Chem. Rev.*, 1999, **99**, 2735–2776.
27 J. A. Jacobsen, J. L. M. Jourden, M. T. Miller and S. M. Cohen, *Biochim. Biophys. Acta Mol. Cell Res.*, 2010, **1803**, 72–94.
28 A. R. Folgueras, A. M. Pendas, L. M. Sanchez and C. Lopez-Otin, *Int. J. Dev. Biol.*, 2004, **48**, 411–424.
29 A.-C. Dublanchet, P. Ducrot, C. Andrianjara, M. O'Gara, R. Morales, D. Compère, A. Denis, S. Blais, P. Cluzeau and K. Courté, *Bioorg. Med. Chem. Lett*, 2005, **15**, 3787–3790.
30 A. R. Johnson, A. G. Pavlovsky, D. F. Ortwine, F. Prior, C.-F. Man, D. A. Bornemeier, C. A. Banotai, W. T. Mueller, P. McConnell, C. Yan, V. Baragi, C. Lesch, W. H. Roark, M. Wilson, K. Datta, R. Guzman, H.-K. Han and R. D. Dyer, *J. Biol. Chem.*, 2007, **282**, 27781–27791.
31 J. J. Li, J. Nahra, A. R. Johnson, A. Bunker, P. O'Brien, W.-S. Yue, D. F. Ortwine, C.-F. Man, V. Baragi and K. Kilgore, *J. Med. Chem.*, 2008, **51**, 835–841.
32 R. Morales, S. Perrier, J.-M. Florent, J. Beltra, S. Dufour, I. De Mendez, P. Manceau, A. Tertre, F. Moreau and D. Compere, *J. Mol. Biol.*, 2004, **341**, 1063–1076.
33 Y. Lyu, Q. Xiao, L. Yin, L. Yang and W. He, *Signal Transduct. Targeted Ther.*, 2019, **4**, 26.
34 T. Fischer and R. Riedl, *Molecules*, 2019, **24**, 2265.
35 L. Devy, L. Huang, L. Naa, N. Yanamandra, H. Pieters, N. Frans, E. Chang, Q. Tao, M. Vanhove and A. Lejeune, *Cancer Res.*, 2009, **69**, 1517–1526.
36 D. C. Marshall, S. K. Lyman, S. McCauley, M. Kovalenko, R. Spangler, C. Liu, M. Lee, C. O'Sullivan, V. Barry-Hamilton and H. Ghermazien, *PLoS One*, 2015, **10**, e0127063.
37 A. Akbarzadeh, R. Khalilov, E. Mostafavi, N. Annabi, E. Abasi, T. Kafshdooz, R. Herizchi, T. Kavetskyy, S. Saghfi and A. Nasibova, *Exp. Oncol.*, 2018, **40**, 178–183.
38 D. A. Fernandes, *J. Bionanosci.*, 2023, **13**, 1609–1644.
39 M. J. Mitchell, M. M. Billingsley, R. M. Haley, M. E. Wechsler, N. A. Peppas and R. Langer, *Nat. Rev. Drug Discovery*, 2021, **20**, 101–124.
40 D. A. Fernandes, *Biomed. Mater. & Devices*, 2024, DOI: **10.1007/s44174-024-00235-8**.
41 D. Huang and D. Wu, *Mater. Sci. Eng. C*, 2018, **90**, 713–727.
42 Y. Tian, M. Sun, R. Song, Z. Yang and H. Zhang, *RSC Adv.*, 2025, **15**, 2981–2987.
43 H. L. Sullivan, Y. Liang, K. Worthington, C. Luo, N. C. Gianneschi and K. L. Christman, *Biomacromolecules*, 2023, **24**, 4695–4704.
44 S. Svenson and A. S. Chauhan, *Nanomedicine*, 2008, **3**, 679–702.
45 J. R. Baker Jr, *Hematology*, 2009, 708–719.
46 X. Zhang, X. Wang, W. Zhong, X. Ren, X. Sha and X. Fang, *Int. J. Nanomed.*, 2016, **11**, 1643–1661.
47 D. Bhunia, K. Pradhan, G. Das, S. Ghosh, P. Mondal and S. Ghosh, *Chem. Commun.*, 2018, **54**, 9309–9312.
48 J. Pan, P.-J. Li, Y. Wang, L. Chang, D. Wan and H. Wang, *Chem. Commun.*, 2018, **54**, 11092–11095.
49 L. Cerofolini, V. Baldoneschi, E. Dragoni, A. Storai, M. Mamusa, D. Berti, M. Fragai, B. Richichi and C. Nativi, *Bioorg. Med. Chem.*, 2017, **25**, 523–527.
50 H. Yao, D. M. Veine, K. S. Fay, E. D. Staszewski, Z.-Z. Zeng and D. L. Livant, *Breast Cancer Res. Treat.*, 2011, **125**, 363–375.
51 Q. Wu, T. Shan, M. Zhao, S. Mai and L. Gu, *R. Soc. Open Sci.*, 2019, **6**, 182104.
52 B. Richichi, V. Baldoneschi, S. Burgalassi, M. Fragai, D. Vullo, A. Akdemir, E. Dragoni, A. Louka, M. Mamusa and D. Monti, *Chem.–Eur. J.*, 2016, **22**, 1714–1721.
53 F. Carta, S. M. Osman, D. Vullo, A. Gullotto, J.-Y. Winum, Z. AlOthman, E. Masini and C. T. Supuran, *J. Med. Chem.*, 2015, **58**, 4039–4045.
54 F. Carta, S. M. Osman, D. Vullo, Z. AlOthman, S. Del Prete, C. Capasso and C. T. Supuran, *Bioorg. Med. Chem.*, 2015, **23**, 6794–6798.
55 F. Carta, S. M. Osman, D. Vullo, Z. AlOthman and C. T. Supuran, *Org. Biomol. Chem.*, 2015, **13**, 6453–6457.
56 S. Svenson and D. A. Tomalia, *Adv. Drug Delivery Rev.*, 2012, **64**, 102–115.
57 R. Kannan, E. Nance, S. Kannan and D. A. Tomalia, *J. Intern. Med.*, 2014, **276**, 579–617.
58 V. Saluja, A. Mankoo, G. K. Saraogi, M. M. Tambuwala and V. Mishra, *J. Drug Delivery Sci. Technol.*, 2019, **52**, 15–26.
59 J. Lim and E. E. Simanek, *Adv. Drug Delivery Rev.*, 2012, **64**, 826–835.
60 H. H. Khalil, H. A. Osman, M. Teleb, A. I. Darwish, M. M. Abu-Serie, S. N. Khattab and N. S. Haiba, *ChemMedChem*, 2021, **16**, 3701–3719.
61 N. S. Haiba, H. H. Khalil, A. Bergas, M. M. Abu-Serie, S. N. Khattab and M. Teleb, *ACS Omega*, 2022, **7**, 21131–21144.
62 H. Huang, *Sensors*, 2018, **18**, 3249.
63 H. Li, Z. Qiu, F. Li and C. Wang, *Oncol. Lett.*, 2017, **14**, 5865–5870.
64 T. I. Huo, H. C. Lin, Y. H. Huang, J. C. Wu, J. H. Chiang, P. C. Lee and S. D. Lee, *Cancer*, 2006, **107**, 141–148.
65 C. Scheau, I. A. Badarau, R. Costache, C. Caruntu, G. L. Mihai, A. C. Didilescu, C. Constantin and M. Neagu, *Anal. Cell. Pathol.*, 2019, **2019**, 9423907.
66 T. Mosmann, *J. Immunol. Methods*, 1983, **65**, 55–63.
67 G. S. Kelly, *Alternative Med. Rev.*, 2011, **16**, 172–195.
68 I. Sarenkova and I. Ciprovica, *Res. Rural Dev.*, 2018, **1**, 233–239.
69 K. K. Selim, Y.-S. Ha, S.-J. Kim, Y. Chang, T.-J. Kim, G. H. Lee and I.-K. Kang, *Biomaterials*, 2007, **28**, 710–716.
70 R. Guo, Y. Yao, G. Cheng, S. H. Wang, Y. Li, M. Shen, Y. Zhang, J. R. Baker, J. Wang and X. Shi, *RSC Adv.*, 2012, **2**, 99–102.
71 A. K. Jangid, S. Kim and K. Kim, *Biomater. Res.*, 2023, **27**, 1–29.
72 G. A. Upadhya and S. M. Strasberg, *Hepatology*, 2000, **31**, 1115–1122.
73 M. Olivieri, M. Cristaldi, S. Pezzino, G. Lupo, C. D. Anfuso, C. Gagliano, C. Genovese and D. Rusciano, *Cornea*, 2018, **37**, 1058–1063.

74 F. M. Veronese and A. Mero, *BioDrugs*, 2008, **22**, 315–329.
75 R. Wang, L. Yang, S. Li, D. Ye, L. Yang, Q. Liu, Z. Zhao, Q. Cai, J. Tan and X. Li, *Med. Sci. Monit.*, 2018, **24**, 412–420.
76 H. Guan, W. Zhang, H. Liu, Y. Jiang, F. Li, M. Wu, G. I. Waterhouse, D. Sun-Waterhouse and D. Li, *Metabolites*, 2023, **13**, 229.
77 O. Nyormoi, L. Mills and M. Bar-Eli, *Cell Death Differ.*, 2003, **10**, 558–569.
78 X. Chen, Z. Zheng, L. Chen and H. Zheng, *Oncotarget*, 2017, **8**, 101452.
79 S. N. Khattab, S. E. Abdel Naim, M. El-Sayed, A. A. El Bardan, A. O. Elzoghby, A. A. Bekhit and A. El-Faham, *New J. Chem.*, 2016, **40**, 9565–9578.
80 D. R. Ramadan, A. A. Elbardan, A. A. Bekhit, A. El-Faham and S. N. Khattab, *New J. Chem.*, 2018, **42**, 10676–10688.
81 Y. E. Jad, S. N. Khattab, B. G. de la Torre, T. Govender, H. G. Kruger, A. El-Faham and F. Albericio, *Eur. J. Org Chem.*, 2015, **2015**, 3116–3120.
82 P. Cherkupally, G. A. Acosta, L. Nieto-Rodriguez, J. Spengler, H. Rodriguez, S. N. Khattab, A. El-Faham, M. Shamis, Y. Luxembourg, R. Prohens, R. Subiros-Funosas and F. Albericio, *Eur. J. Org Chem.*, 2013, **2013**, 6372–6378.
83 S. N. Khattab, *Chem. Pharmaceut. Bull.*, 2010, **58**, 501–506.
84 L. Shi, J. Zhang, M. Zhao, S. Tang, X. Cheng, W. Zhang, W. Li, X. Liu, H. Peng and Q. Wang, *Nanoscale*, 2021, **13**, 10748–10764.
85 J. V. Jokerst, T. Lobovkina, R. N. Zare and S. S. Gambhir, *Nanomedicine*, 2011, **6**, 715–728.
86 O. R. M. Metawea, M. Teleb, N. S. Haiba, A. O. Elzoghby, A. F. Khafaga, A. E. Noreldin, S. N. Khattab and H. H. Khalil, *Eur. Polym. J.*, 2023, **182**, 111721.
87 M. Gaber, K. A. Elhasany, S. Sabra, M. W. Helmy, J.-Y. Fang, S. N. Khattab, A. A. Bekhit, M. Teleb, K. A. Elkodairy and A. O. Elzoghby, *Colloids Surf., B*, 2020, **192**, 110997.
88 K. A. Elhasany, S. N. Khattab, A. A. Bekhit, D. M. Ragab, M. A. Abdulkader, A. Zaky, M. W. Helmy, H. M. Ashour, M. Teleb and N. S. Haiba, *Eur. J. Pharm. Biopharm.*, 2020, **155**, 162–176.
89 Y. Cao, R. A. DePinho, M. Ernst and K. Vousden, *Nat. Rev. Cancer*, 2011, **11**, 749–754.
90 C. Munaut, A. Noël, O. Hougrand, J.-M. Foidart, J. Boniver and M. Deprez, *Int. J. Cancer*, 2003, **106**, 848–855.
91 Molecular Operating Environment (MOE), *102 Chemical Computing Group ULC*, Montreal, QC, Canada, 2019.
92 S. Rowsell, P. Hawtin, C. A. Minshull, H. Jepson, S. M. Brockbank, D. G. Barratt, A. M. Slater, W. L. McPheat, D. Waterson, A. M. Henney and R. A. Pauptit, *J. Mol. Biol.*, 2002, **319**, 173–181.